

# PO-Flow: Flow-based Generative Models for Sampling Potential Outcomes and Counterfactuals

Dongze Wu\*, David I. Inouye†, Yao Xie\*

## Abstract

Predicting potential and counterfactual outcomes from observational data is central to clinical decision-making, where physicians must weigh treatments for an individual patient rather than relying solely on average effects at the population level. We propose PO-Flow, a continuous normalizing flow (CNF) framework for causal inference that jointly models potential outcomes and counterfactuals. Trained via flow matching, PO-Flow provides a unified approach to average treatment effect estimation, individualized potential outcome prediction, and counterfactual prediction. Besides, PO-Flow directly learns the densities of potential outcomes, enabling likelihood-based evaluation of predictions. Furthermore, PO-Flow explores counterfactual outcome generation conditioned on the observed factual in general observational datasets, with a supporting recovery result under certain assumptions. PO-Flow outperforms modern baselines across diverse datasets and causal tasks in the potential outcomes framework.

## 1 Introduction

Predicting potential outcomes (POs) lies at the core of causal inference. In a typical setting, each individual has two potential outcomes:  $Y^{(1)}$  if they receive a treatment ( $A = 1$ ) and  $Y^{(0)}$  if they do not ( $A = 0$ ). However, in the real world, only one outcome is observed, while the other potential outcome remains fundamentally unknown [25]. Accurately estimating both POs is crucial for decision-making in healthcare [37, 24, 46], where clinicians may wish to compare a patient’s likely outcomes under different treatment options rather than rely solely on average effects [56, 17].

In the Potential Outcomes (POs) literature, the vast majority of methods focus on estimating the conditional average treatment effect (CATE):  $\mathbb{E}[Y^{(1)} - Y^{(0)}|X]$ , at the population level [28, 22, 1, 19, 33, 38, 50, 61]. It is important to note that although some methods perform well in estimating population-level CATE, they may underperform in individualized POs prediction, as accurately predicting POs in finite samples is challenging [47].

However, making decisions for individuals based on average treatment effects can be misleading. Therefore, accurately predicting individualized POs and learning their full distributions  $p(Y^{(A)}|X, A)$  is a crucial task [63, 31]. Recent works [61, 40, 41] have explored generative models to sample POs and estimate empirical distributions. However, methods that learn the full density of POs without relying on explicit distributional assumptions (e.g., Gaussian mixtures) remain scarce.

In addition, another critical challenge is estimating the counterfactual outcome conditioned on the factual:  $Y_{CF}^{(1-A)} := Y^{(1-A)}|X, Y^{(A)}$ , i.e., predicting what would have happened under the

---

\*H. Milton Stewart School of Industrial and Systems Engineering, Georgia Institute of Technology, Atlanta, GA 30332. <dwu381@gatech.edu> <yao.xie@isye.gatech.edu>

†Elmore Family School of Electrical and Computer Engineering, Purdue University, West Lafayette, IN 47907. <dinouye@purdue.edu>

alternative treatment, given the observed outcome  $Y^{(A)}$ . This task is especially relevant in post-hoc clinical analyses, where practitioners ask, “Would the patient have fared better on another therapy?” [60, 18].

Counterfactual prediction differs from standard PO estimation—it requires reasoning about outcomes under an alternative treatment *conditioned on the observed factual outcome*, introducing dependencies between observed and unobserved outcomes. Structural Causal Models (SCMs) [44] and modern extensions [42, 6, 12, 7, 59, 45, 8] offer the most widely used theoretical framework for counterfactual reasoning. SCMs methods typically assume known causal structures or aim to learn them explicitly. However, it may be possible to estimate counterfactuals directly without recovering the SCM [64]. In PO-Flow, we do not explicitly assume an SCM, but seek to directly estimate counterfactual outcomes.

Despite recent progress, two key gaps remain in the potential outcomes literature. First, counterfactual outcome estimation conditioned on the observed factual outcome has received little attention, though it is crucial for post-hoc analyses. Second, beyond counterfactuals, most methods are specialized—some target CATE estimation, others aim at potential outcome prediction or distributional modeling—but few provide a unified and scalable algorithmic framework that can jointly address these tasks.

## 1.1 Main Contributions

We propose PO-Flow, a continuous normalizing flow (CNF) framework for potential outcomes and counterfactuals. Our **main contributions** are: (1) Enable counterfactual outcome generation conditioned on the observed factual, together with a supporting counterfactual recovery result (Corollary 4.5) under certain assumptions; (2) Provide a unified generative framework for potential outcome prediction, CATE estimation, and general-purpose counterfactual prediction; (3) Learn the density of potential outcomes, supporting principled uncertainty quantification; (4) Achieve superior performance over state-of-the-art methods across diverse causal tasks and benchmark datasets.

## 1.2 Related Works

*CATE Estimation:* Numerous methods have been proposed for CATE estimation [28, 22, 1, 19, 33, 38, 50, 61]. Broadly, these fall into model-agnostic and model-specific approaches. Model-agnostic estimators, or meta-learners [33, 15, 14, 2, 49], typically follow two strategies [39]: (a) one-step methods, which fit regression models and compute CATE as the difference in predicted outcomes, and (b) two-step methods, which estimate nuisance functions to construct pseudo-outcomes, then regress them on covariates.

In contrast, model-specific estimators adapt machine learning techniques for CATE estimation, including methods such as [13, 50, 38, 30, 61]. More recently, neural networks have been widely applied to this task, with notable examples in [50, 38, 61]. However, most of these approaches mainly focus on estimating CATE rather than predicting individualized potential outcomes.

*Individualized POs Prediction:* Although some CATE methods can be adapted for potential outcomes (POs) prediction, they may perform suboptimally, particularly on finite samples, as they are not specifically optimized for accurate PO estimation. This limitation partly arises because many methods assume that CATE has a simpler functional structure than POs. Nevertheless, several CATE approaches are also designed with POs prediction as the target [33, 50, 61, 38, 41, 39].

*Counterfactual Outcomes Prediction:* Structural Causal Models (SCMs) provide a well-established framework for counterfactual reasoning [44, 42, 6, 12, 7, 59, 45, 8], but practical applications often require specifying the full causal graph and structural equations, which may be difficult or infeasible for real-world data. Some recent works avoid explicitly modeling SCMs [35, 5, 40, 57], but typically address specific tasks and rely on additional information, such as temporal structure.

Some works [24, 30, 38, 34, 61] targeting CATE estimation describe their goal as counterfactual inference. However, in these works, "counterfactual" typically refers to the unobserved potential outcome under an alternative treatment, without conditioning on the observed factual outcome.

While SCMs offer theory-grounded counterfactual reasoning, general-purpose methods for individualized counterfactual prediction—without explicitly modeling SCMs or relying on auxiliary information—remain scarce. Although [61, 39] were not originally designed for counterfactuals, we can adapt them by incorporating factual information into intermediate steps and use them as baselines.

*Diffusion and Flow Models:* Diffusion models [23, 52, 54] and flow-based generative models [10, 58, 36, 4] have demonstrated strong performance across a range of applications. Recently, diffusion and flow-based generative models have been applied to causal inference tasks such as counterfactual image generation [48, 16], causal query answering [9], and inference over causal graphs or structural causal models [8, 29]. To our knowledge, two generative algorithms have been proposed specifically for the potential outcomes (PO) task: the diffusion-based DiffPO [39] and the discrete normalizing flow-based INFs [41]. We conduct extensive comparisons with both methods in this work.

## 2 Preliminaries

### 2.1 Neural ODE and Continuous Normalizing Flow:

A Neural ODE is a continuous model where the trajectory of data is modeled as the solution of an ordinary differential equation (ODE). Formally, in  $\mathbb{R}^d$ , given an input  $y_0 = y(0)$  at time  $t = 0$ , the transformation to the output  $y_1 = y(1)$  at time  $t = 1$  is governed by:

$$\frac{dy(t)}{dt} = v_\theta(y(t), t), \quad t \in [0, 1], \quad (1)$$

where  $v_\theta : \mathbb{R}^d \times [0, 1] \rightarrow \mathbb{R}^d$  represents the velocity field, which is parameterized by a neural network with parameter  $\theta$ . The time horizon is rescaled to  $[0, 1]$  without loss of generality.

Continuous Normalizing Flow (CNF) is a class of normalizing flows in which the transformation of a probability density is governed by a time-continuous Neural ODE. The marginal density of  $y(t)$ , denoted as  $p(y, t)$ , evolves according to the continuity equation implied by the ODE in Eq. (1). This continuity equation is given by:

$$\partial_t p(y, t) + \nabla \cdot (p(y, t)v_\theta(y, t)) = 0, \quad t \in [0, 1], \quad (2)$$

where  $\nabla \cdot$  denotes the divergence operator.

When the Neural ODE is well-posed, it defines a continuous and invertible mapping from the initial sample  $y_0$  to the terminal sample  $y_1$ . The inverse mapping from  $y_1$  to  $y_0$  can be computed by integrating the ODE (1) in reverse time.

This framework allows setting  $y_0 \sim p(\cdot, 0)$  as the data distribution and  $y_1 \sim p(\cdot, 1)$  as the base (noise) distribution, typically chosen as  $N(0, I)$ . For notational convenience, we define  $p_Y(\cdot) := p(\cdot, 0)$  as the data distribution and  $q(\cdot) := p(\cdot, 1)$  as the base (noise) distribution. Throughout this paper, we adopt the common choice  $q(\cdot) = N(0, I)$ .

### 2.2 Flow Matching

Flow Matching (FM) [36, 4] provides a simulation-free approach for training continuous normalizing flows by directly regressing the model velocity  $v_\theta(y, t)$  onto a predefined target velocity field

$u(y, t)$ . The original FM objective is defined as:

$$\mathcal{L}_{\text{FM}}(\theta) = \mathbb{E}_{t \sim \mathcal{U}[0,1], y \sim p(\cdot, t)} [\|v_\theta(y, t) - u(y, t)\|^2], \quad (3)$$

where  $u(y, t)$  is an analytically specified target velocity field.

**Linear Interpolant:** Due to the intractability of  $u(y, t)$  without conditioning on the initial data  $y_0$ , Conditional Flow Matching (CFM) is introduced. Conditioned on an observed sample  $y_0 \sim p_Y(\cdot)$ , CFM employs a pre-specified interpolation function  $I_t$  between two endpoints  $y_0$  and  $y_1 \sim q(\cdot)$ , where  $q$  is typically  $N(0, I)$ . The interpolated path is defined as:

$$\phi(y_0, y_1; t) := I_t(y_0, y_1), \quad t \in [0, 1]. \quad (4)$$

Here,  $I_t$  can be analytically specified. Conditioned on  $y_0$ , the optimal and most information-preserving choice is the linear interpolation path [36]:

$$\phi(y_0, y_1; t) = (1 - t)y_0 + (t + \sigma_{\min}(1 - t))y_1, \quad (5)$$

where  $y_1 \sim N(0, I)$  and  $\sigma_{\min}$  is a small positive hyperparameter that ensures  $p(\phi, 0) \sim N(y_0, \sigma_{\min}^2 I)$ . When  $\sigma_{\min} = 0$ , this reduces to the strict linear interpolant  $\phi = (1 - t)y_0 + ty_1$ .

Here,  $\phi$  serves as a pre-specified reference trajectory that the ODE solution  $y(t)$  should follow at time  $t$ . Under the linear interpolant defined in (5), the corresponding reference velocity field becomes:

$$\frac{d\phi}{dt} = (1 - \sigma_{\min})y_1 - y_0. \quad (6)$$

**Training loss:** CFM trains the flow  $v_\theta(y(t), t)$  by directly regressing it onto the reference velocity field (6). The training objective is given by:

$$\mathcal{L}_{\text{CFM}}(\theta) = \mathbb{E}_{t \sim \mathcal{U}[0,1], y_0 \sim p_Y(\cdot), y_1 \sim q(\cdot)} \|v_\theta(\phi, t) - \frac{d\phi}{dt}\|^2. \quad (7)$$

### 3 Problem Settings

**Notations and Setups:** We consider a setting where each individual is described by covariates  $X \in \mathbb{R}^{d_X}$ , a treatment assignment  $A \in \{0, 1\}$ , and a potential outcome  $Y^{(A)} \in \mathbb{R}$  under treatment  $A$ . The observational dataset is  $\mathcal{D} = \{(y_i^{(a)}, x_i, a_i)\}_{i=1}^n \sim p_{Y, X, A}(\cdot)$ , where  $y_i^{(a)}$  is the observed potential outcome under treatment  $a_i$ , and  $(x_i, a_i) \sim p_{X, A}(\cdot)$  are the associated covariates and treatment.

**Potential Outcomes:** In the potential outcomes framework, each individual has two potential outcomes:  $Y^{(0)}$  (control) and  $Y^{(1)}$  (treatment), but only one is observed based on assignment  $A$ . We define potential outcome prediction as estimating  $Y^{(a)} \mid X, A = a$ . For convenience, we denote  $Y^{(a)}$  and  $\hat{Y}^{(a)}$  as the true and predicted potential outcomes.

**Counterfactual Outcomes:** In contrast to potential outcomes, we define the counterfactual outcome as  $Y_{\text{cf}}^{(1-a)} := Y^{(1-a)} \mid X, A = a, Y^{(a)}$ , which is the outcome had the individual received the opposite treatment, conditioned on its observed potential (factual) outcome. For convenience, we denote  $Y_{\text{cf}}^{(1-a)}$  and  $\hat{Y}_{\text{cf}}^{(1-a)}$  as the true and predicted counterfactual outcomes, respectively.

To ensure the identifiability of potential outcomes (in Section 4.1), we adopt the standard assumptions commonly used in the literature [39, 41, 61]:

**Assumption 3.1.** (1) Consistency: If an individual receives treatment  $A = a$ , the observed outcome equals the corresponding potential outcome:  $Y = Y^{(a)}$ . (2) Unconfoundedness: All confounders are observed, i.e.,  $\{Y^{(0)}, Y^{(1)}\} \perp\!\!\!\perp A \mid X$ . (3) Overlap: Treatment assignment is probabilistic:  $0 < P(A = 1 \mid X = x) < 1$ , for all  $x \in \mathcal{X}$ .

In Section 4.2, we will introduce additional assumptions on counterfactual outcomes estimation in PO-Flow and provide the corresponding theoretical analyses for counterfactual recovery.

## 4 PO-Flow: A Continuous Normalizing Flow for Potential Outcomes

We introduce PO-Flow, a continuous normalizing flow framework for modeling potential and counterfactual outcomes, with three main goals: 1. predicting individualized potential outcomes, 2. predicting counterfactual outcomes, and 3. learning the densities.

Our PO-Flow framework is built on Continuous Normalizing Flows (CNFs) and is trained using the Flow Matching (FM) objective. Our learning target is the trajectory of the sample  $y(t)$  over  $t \in [0, 1]$ . To condition the dynamics on both covariates  $x$  and treatment  $a$ , the Neural ODE is defined as:

$$\frac{dy(t)}{dt} = v_\theta(y(t), t; x, a), \quad t \in [0, 1], \quad (8)$$

where  $v_\theta$  is parametrized by a neural network, with  $y(0)$  following the data distribution and  $y(1) \sim q(\cdot)$ .

**Notation:** Given a data point  $(y^{(a)}, x, a) \sim p_{Y, X, A}(\cdot)$ , we define  $y_0 = y^{(a)}$  as the observed training sample at time  $t = 0$  in the Neural ODE, and  $y_1 \sim q(\cdot)$  as the noise sample at time  $t = 1$ . Recall that we denote  $\hat{y}^{(a)}$  and  $\hat{y}_{\text{cf}}^{(1-a)}$  as the predicted potential and counterfactual outcomes, respectively.

**Training loss:** PO-Flow adopts the Conditional Flow Matching (CFM) objective for training. Under the updated definitions, our training loss retains the form of Equation (7) and is given by:

$$\min_{\theta} \mathcal{L}_{\text{CFM}}(\theta) = \mathbb{E}_{t \sim \mathcal{U}[0, 1], p_{Y, X, A}(\cdot), q(\cdot)} \|v_\theta(\phi, t; x, a) - \frac{d\phi}{dt}\|^2, \quad (9)$$

where  $\phi$  and  $\frac{d\phi}{dt}$  are defined in (5) and (6), respectively, with  $y_0 = y^{(a)}$  and  $y_1 \sim q(\cdot)$ .

*Remark:* Following prior works [20, 39], one may estimate propensity scores  $w(x) = p(A = 1 | X = x)$  with a pre-trained classifier and apply inverse weighting  $\frac{1}{w(x)}$  in the loss. We found this provided little performance improvement, but both implementations are included in our code.

**Forward Process:** We treat the forward process as an encoding operation, denoted by the function  $Z := \Phi_\theta(Y^{(A)}; X, A)$ . Given the velocity field  $v_\theta$ , the forward process refers to pushing a factual outcome  $y^{(a)}$  (at  $t = 0$ ) to a latent embedding  $z$  (at  $t = 1$ ) via:

$$z := \Phi_\theta(y^{(a)}; x, a) = y^{(a)} + \int_0^1 v_\theta(y(t), t; x, a) dt, \quad \text{with } y(0) = y^{(a)}. \quad (10)$$

Through the forward process,  $z$  encodes information from the factual outcome  $y^{(a)}$  as well as its associated covariates  $x$  and treatment  $a$ .

**Reverse Process:** We treat the reverse process as a decoding operation. It is initialized differently for potential outcome (Section 4.1) and counterfactual prediction (Section 4.2). In general, at  $t = 1$ , given a latent representation  $z$ , which can be either sampled from  $q(\cdot) = N(0, 1)$  or obtained by encoding a factual sample, the reverse process is defined as:

$$\hat{y}_0 := \Phi_\theta^{-1}(z; x, a) = z - \int_0^1 v_\theta(y(t), t; x, a) dt, \quad \text{with } y(1) = z. \quad (11)$$

Empirically, we use the Runge-Kutta method (Appendix B.3) for numerical integration.

During training, we construct synthetic paths  $\phi$  between  $y_0$  and  $y_1 \sim q(\cdot)$  using the CFM loss conditioned on  $y_0$ . As shown in Proposition A.1 (Appendix), the gradient of the CFM loss is equivalent to that of the original FM loss. Consequently, the learned velocity field  $v_\theta$  generates  $\hat{y}_0$  independent of the specific training samples  $y_0$ , and since  $y_1 \sim q(\cdot)$  is random,  $v_\theta$  induces a distribution over outcomes conditioned on  $(x, a)$ .

---

**Algorithm 1:**Potential Outcomes Prediction

---

**Require:** Trained  $v_\theta$ **Input:**  $(x, a) \sim p_{X,A}(\cdot)$ 1:  $z \sim q(\cdot)$ 2:  $\hat{y}_0 = z - \int_0^1 v_\theta(y(t), t; x, a) dt$ **Return:**  $\hat{y}^{(a)} := \hat{y}_0$ 

---

#### 4.1 PO-Flow for Potential Outcomes Prediction

To sample potential outcomes  $\hat{y}^{(a)}$  for an individual  $(x, a)$ , the procedure follows a simple reverse process, as defined in Equation (11). Starting from a noise sample  $z \sim q(\cdot)$ , we integrate the velocity field  $v_\theta$  backward in time, conditioned on covariates  $x$  and treatment  $a$ , to obtain a point estimate of the potential outcome  $\hat{y}^{(a)}$ . The steps are summarized in Algorithm 1.

In addition to predicting point estimates of potential outcomes, PO-Flow is capable of learning the densities of the potential outcomes, as detailed in Section 4.3.

#### 4.2 PO-Flow for Counterfactual Outcomes Prediction

The counterfactual outcome prediction consists of both a forward and a reverse process. Given a factual  $(y^{(a)}, x, a) \sim p_{Y,X,A}(\cdot)$ , the forward process (Lines 1–2 in Alg. 2) encodes  $(y^{(a)}, x, a)$  into a latent representation  $z$ . Subsequently, the reverse process (Lines 3–5) decodes  $z$  under the counterfactual treatment  $1 - a$ , yielding the counterfactual prediction  $\hat{y}_{cf}^{(1-a)}$ . The process of counterfactual prediction is also illustrated in Figure 1.

---

**Algorithm 2:**Counterfactual Prediction

---

**Require:** Trained  $v_\theta$ **Input:** Factual sample  $(y^{(a)}, x, a) \sim p_{Y,X,A}(\cdot)$ 

1. Forward process {abduction}:

2.  $z = y^{(a)} + \int_0^1 v_\theta(y(t), t; x, a) dt$ ,  
with  $y(0) = y^{(a)}$ .

3. Reverse process {action and prediction}:

4. Set intervened action to  $1 - a$ ;5.  $\hat{y}_0 = z - \int_0^1 v_\theta(y(t), t; x, 1 - a) dt$ ,  
with  $y(1) = z$ .**Return:**  $\hat{y}_{cf}^{(1-a)} := \hat{y}_0$ 

---

Because of the smooth and information-preserving nature of the continuous normalizing flow path, the encoded  $z$  retains rich information from the factual outcome  $y^{(a)}$ , enabling accurate decoding of the counterfactual  $\hat{y}_{cf}^{(1-a)}$  under counterfactual treatment  $1 - a$ . To our knowledge, this work is among the early attempts at counterfactual prediction in the Potential Outcomes (POs) literature.

In the following, we present a supporting result on the counterfactual recovery properties of PO-Flow under monotone structural causal models (SCMs). While PO-Flow does not explicitly aim to model the true SCM during training or inference, we show that if the data are generated from monotone SCMs, then PO-Flow provides recovery guarantees under certain conditions.

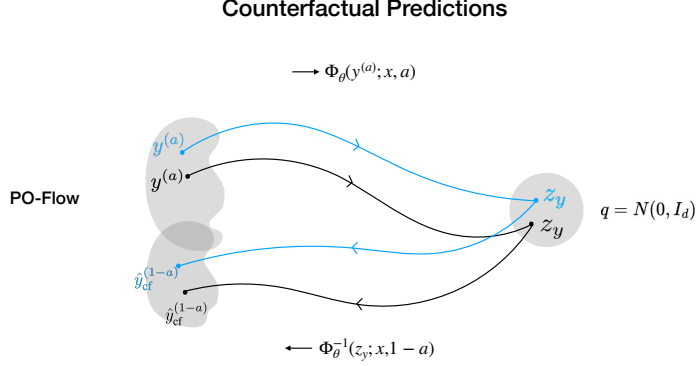


Figure 1: Illustration of counterfactual predictions. *Left*: two potential outcomes distribution. *Right*: base (noise) distribution.

We denote the SCM for an individual as  $Y^{(A)} = f_X(A, U)$ , where  $U$  denotes the exogenous noise. The encoding function is given by  $Z := \Phi_\theta(Y^{(A)}; X, A)$ , which corresponds to Equation (10). We begin by introducing the following assumptions:

**Assumption 4.1.**

(A1)  $U \perp\!\!\!\perp A$ .

(A2) The structural causal model  $f_X(A, U)$  is monotone in  $U$  for each action  $A \in \{0, 1\}$ .

(A3) For every  $x$ , the encoded latent  $Z = \Phi_\theta(Y^{(A)}; X, A)$  induced by the flow is statistically independent of  $A$ , i.e.,  $Z \perp\!\!\!\perp A \mid X = x$ .

**Remark 4.2.** In the POs framework, covariates  $x$  are multivariate while the potential outcome is univariate,  $y \in \mathbb{R}$ . Therefore, (A2) is invoked for the univariate case. It is automatically satisfied under an additive structural causal model,  $Y^{(A)} = f_X(A, U) := f_X^*(A) + U$ . Under certain identifiability conditions, it also holds for non-linear models [62, 55]. The following theoretical results hold only under monotone SCM settings.

(A3) assumes the encoded representation  $Z = \Phi_\theta(Y^{(A)}; X, A)$  in PO-Flow is statistically independent of treatment  $A$ , though not necessarily functionally invariant to  $A$ . In the infinite-data limit with exact training, the continuous normalizing flow (Equation (8)) maps each treatment-conditioned outcome  $Y$  to the same base distribution  $q(Z) = \mathcal{N}(0, 1)$ , so  $p_\theta(Z \mid X, A) = q(Z)$  and (A3) holds exactly. In finite samples, deviations may arise; we assess this empirically in Appendix D.1.

Under the Assumption 4.1, we present a result for PO-Flow when the true SCM is monotone:

**Proposition 4.3** (Encoded  $Z$  as a function of the exogenous noise  $U$ ). *Let Assumption 4.1 hold. Assume that the exogenous noise  $U \sim \text{Unif}[0, 1]$ . Then there exists a continuously differentiable bijection function  $\psi_X : \mathcal{U} \rightarrow \mathcal{Z}$  that is independent of the treatment assignment  $A$ , i.e.,*

$$Z = \Phi_\theta(Y^{(A)}; X, A) = \Phi_\theta(f_X(A, U); X, A) = \psi_X(U) \tag{12}$$

**Remark 4.4.** We can transform the exogenous noise  $U \sim \text{Unif}[0, 1]$  assumed in Proposition 4.3 into other distributions, such as Gaussian. If  $Z \sim \mathcal{N}(0, 1)$  with CDF  $F(Z)$ , then  $U = F(Z) \sim \text{Unif}[0, 1]$ , and any structural assignment  $f(\cdot, U)$  can be written equivalently as  $f(\cdot, Z) = f(\cdot, F(Z))$ . Therefore, the conclusions of Proposition 4.3 also hold with other noise distributions.

Following Proposition 4.3, we have the following result on counterfactual recovery under monotone SCMs:

**Corollary 4.5** (Counterfactual recovery under monotone SCMs). *Assume the conditions in Assumption 4.1 hold. Consider a factual sample  $(Y^{(A)}, X, A)$  given by the structural equation  $Y^{(A)} = f_X(A, U)$ , and let its encoded representation be  $Z = \Phi_\theta(Y^{(A)}; X, A)$ . Apply the intervention  $\text{do}(A = \gamma)$ . Assume that the true counterfactual is given by  $Y_{\text{CF}}^{(\gamma)} = f_X(\gamma, U)$ . The decoder then recovers the counterfactual almost surely:*

$$\hat{Y}_{\text{CF}}^\gamma := \Phi_\theta^{-1}(Z; X, \gamma) = Y_{\text{CF}}^\gamma. \quad (13)$$

**Remark 4.6.** One may notice that Assumptions (A1) and (A2) mirror those in Bijective Generation Mechanisms (BGM) [43]. BGM establishes class-level identifiability: if a learned mechanism lies in the BGM class and matches the observational distribution ( $\hat{f}_X(A, U) \stackrel{d}{=} f_X(A, U)$ ), then counterfactuals are identifiable. By contrast, our Prop. 4.3 shows that PO-Flow’s encoder is bijective in  $U$ , placing our model within the BGM class. We then use an alternative constructive route (building on the intermediate step in Prop. 4.3) to obtain Cor. 4.5 under (A1)–(A3). Alternatively, one could invoke the BGM result after Prop. 4.3 to reach Cor. 4.5; see Appendix C.

### 4.3 PO-Flow for Learning Potential Outcomes Densities

Another advantage of PO-Flow is its ability to learn the density of the Potential Outcomes (POs). We define  $p_{\theta, Y|X, A}(\cdot | x, a, z)$  as the PO density computed by PO-Flow, conditioned on  $(x, a)$  and a base sample  $z$ . The explicit form of this density, mapping from latent to data space, is presented in Proposition 4.7, with the proof provided in Appendix A.

**Proposition 4.7.** *Given a noise sample  $z \sim q(\cdot)$  at  $t = 1$ , the log-density of the resulting potential outcome at  $t = 0$ , obtained via PO-Flow, is given by:*

$$\log p_{\theta, Y|X, A}(y(0) | x, a, z) = \log q(z) + \int_0^1 \nabla_y \cdot v_\theta(y(t), t; x, a) dt. \quad (14)$$

Empirically, the divergence of the velocity field can be computed much more efficiently under the Hutchinson trace estimator (e.g., [27, 58]). More details are provided in Appendix B.4.

Unlike prior works [40, 41] that generate PO samples and approximate empirical distributions, PO-Flow provides direct likelihood evaluation. This allows principled uncertainty quantification, supports ranking outcomes by plausibility (Table 4), enables information-theoretic analyses such as KL divergence (Table 3), and facilitates tasks like anomaly detection via quantile-based thresholds.

## 5 Experiments

*Baselines:* Our baselines cover several categories: model-agnostic learners that learn the conditional distribution means (S-learner [33], T-learner [33], and DR-Learner [32]), representation-based conditional regressors (Counterfactual Regression (CFR) [50]), deep generative methods (Causal Effect Variational Autoencoder (CEVAE) [38]; GAN for Individualized Treatment Effect (GANITE) [61]), and most recent generative approaches based on diffusion (DiffPO [39]) and discrete normalizing flows (INFs [41]).

*Datasets:* Counterfactual outcomes and unobserved potential outcomes (POs) are inaccessible in real-world data but can be simulated in semi-synthetic settings, as discussed in detail in Appendix B.1. Accordingly, we evaluate PO-Flow on synthetic benchmarks, including ACIC 2016, ACIC 2018, IHDP, and IBM.

The code and datasets are included in the supplementary materials for anonymous submission.

## 5.1 Prediction of Potential Outcomes

Table 1: Root mean squared error (RMSE) of estimated potential outcomes (POs) across different methods on the ACIC 2018, IHDP, and IBM datasets. Results are averaged over 10-fold cross-validation.

	ACIC 2018		IHDP		IBM	
	RMSE <sub>in</sub>	RMSE <sub>out</sub>	RMSE <sub>in</sub>	RMSE <sub>out</sub>	RMSE <sub>in</sub>	RMSE <sub>out</sub>
<b>PO-Flow</b>	<b>0.53<sub>±.10</sub></b>	0.60 <sub>±.12</sub>	<b>0.98<sub>±.11</sub></b>	<b>1.19<sub>±.13</sub></b>	<b>0.90<sub>±.09</sub></b>	<b>0.97<sub>±.11</sub></b>
DiffPO	0.72 <sub>±.14</sub>	0.79 <sub>±.16</sub>	1.33 <sub>±.20</sub>	1.40 <sub>±.22</sub>	1.82 <sub>±.38</sub>	1.85 <sub>±.35</sub>
INFs	0.69 <sub>±.16</sub>	0.78 <sub>±.17</sub>	1.02 <sub>±.10</sub>	<b>1.20<sub>±.12</sub></b>	1.52 <sub>±.24</sub>	1.57 <sub>±.28</sub>
S-learner	<b>0.54<sub>±.09</sub></b>	<b>0.57<sub>±.11</sub></b>	1.31 <sub>±.18</sub>	1.44 <sub>±.20</sub>	1.01 <sub>±.17</sub>	1.16 <sub>±.19</sub>
T-learner	1.57 <sub>±.32</sub>	1.71 <sub>±.40</sub>	1.45 <sub>±.25</sub>	1.49 <sub>±.27</sub>	1.89 <sub>±.47</sub>	1.96 <sub>±.50</sub>
CEVAE	0.83 <sub>±.17</sub>	0.85 <sub>±.17</sub>	1.18 <sub>±.15</sub>	1.36 <sub>±.18</sub>	0.96 <sub>±.12</sub>	<b>0.98<sub>±.12</sub></b>
CFR	0.94 <sub>±.10</sub>	0.98 <sub>±.12</sub>	1.10 <sub>±.20</sub>	<b>1.18<sub>±.20</sub></b>	2.09 <sub>±.45</sub>	2.17 <sub>±.48</sub>
GANITE	0.88 <sub>±.15</sub>	0.97 <sub>±.15</sub>	1.60 <sub>±.36</sub>	1.67 <sub>±.34</sub>	2.48 <sub>±.39</sub>	2.59 <sub>±.47</sub>

*Evaluation Metrics:* We evaluate the point estimates of potential outcomes (POs) using the root mean squared error (RMSE) between the estimated outcomes  $\hat{y}_i^{(a)}$  and the true outcomes  $y_i^{(a)}$ , computed as  $\text{RMSE} = \sqrt{\frac{1}{n} \sum_{i=1}^n (y_i^{(a)} - \hat{y}_i^{(a)})^2}$ , where  $\text{RMSE}_{\text{in}}$  and  $\text{RMSE}_{\text{out}}$  refer to the RMSE evaluated on the training and test sets, respectively.

*Results:* Table 1 shows that PO-Flow achieves the most accurate prediction of potential outcomes on the majority of datasets.

Besides, we also report in Table 4 the RMSE of the most likely POs selected by PO-Flow using the highest log-density (as computed in Proposition 4.7).

## 5.2 Estimation of CATEs

*Conditional Average Treatment Effect (CATE):* The CATE is defined as  $\tau(x) = \mathbb{E}[y^{(a=1)} - y^{(a=0)} | X = x]$ , representing the expected treatment effect conditioned on covariates  $x$ . It captures individual-level heterogeneity in causal effects.

*Evaluation Metrics:* We evaluate CATE using the precision in estimation of heterogeneous effect (PEHE), defined as the mean squared error between estimated and true effects:  $\epsilon_{\text{PEHE}} = \frac{1}{n} \sum_{i=1}^n (\hat{\tau}(x_i) - \tau(x_i))^2$ . Table 2 reports the root PEHE for both training and test sets. PO-Flow achieves the most accurate CATE estimates on most datasets.

Table 2: Root Precision in Estimation of Heterogeneous Effect ( $\sqrt{\epsilon_{\text{PEHE}}}$ ) across different methods on the ACIC 2016, ACIC 2018, IHDP, and IBM datasets.

	ACIC 2016		ACIC 2018		IHDP		IBM	
	$\sqrt{\epsilon_{\text{PEHE}}^{\text{in}}}$	$\sqrt{\epsilon_{\text{PEHE}}^{\text{out}}}$	$\sqrt{\epsilon_{\text{PEHE}}^{\text{in}}}$	$\sqrt{\epsilon_{\text{PEHE}}^{\text{out}}}$	$\sqrt{\epsilon_{\text{PEHE}}^{\text{in}}}$	$\sqrt{\epsilon_{\text{PEHE}}^{\text{out}}}$	$\sqrt{\epsilon_{\text{PEHE}}^{\text{in}}}$	$\sqrt{\epsilon_{\text{PEHE}}^{\text{out}}}$
<b>PO-Flow</b>	<b>0.76<sub>±.08</sub></b>	<b>0.82<sub>±.09</sub></b>	<b>0.05<sub>±.01</sub></b>	<b>0.07<sub>±.02</sub></b>	<b>0.41<sub>±.08</sub></b>	<b>0.45<sub>±.10</sub></b>	<b>0.04<sub>±.01</sub></b>	<b>0.04<sub>±.01</sub></b>
DiffPO	0.91 <sub>±.20</sub>	1.12 <sub>±.26</sub>	0.07 <sub>±.03</sub>	<b>0.08<sub>±.04</sub></b>	0.79 <sub>±.16</sub>	0.84 <sub>±.18</sub>	0.08 <sub>±.03</sub>	0.09 <sub>±.03</sub>
INFs	1.37 <sub>±.28</sub>	1.42 <sub>±.30</sub>	0.33 <sub>±.11</sub>	0.37 <sub>±.12</sub>	0.90 <sub>±.27</sub>	0.95 <sub>±.27</sub>	0.16 <sub>±.08</sub>	0.18 <sub>±.08</sub>
S-learner	3.81 <sub>±.76</sub>	3.87 <sub>±.98</sub>	<b>0.06<sub>±.02</sub></b>	<b>0.07<sub>±.03</sub></b>	0.92 <sub>±.07</sub>	0.93 <sub>±.08</sub>	0.06 <sub>±.02</sub>	0.07 <sub>±.04</sub>
T-learner	5.02 <sub>±.71</sub>	5.15 <sub>±.87</sub>	1.21 <sub>±.47</sub>	1.32 <sub>±.53</sub>	1.24 <sub>±.08</sub>	1.31 <sub>±.09</sub>	0.60 <sub>±.14</sub>	0.69 <sub>±.15</sub>
DR-learner	3.04 <sub>±.19</sub>	3.51 <sub>±.23</sub>	0.43 <sub>±.08</sub>	0.57 <sub>±.10</sub>	1.03 <sub>±.09</sub>	1.28 <sub>±.15</sub>	0.12 <sub>±.03</sub>	0.19 <sub>±.05</sub>
CEVAE	2.06 <sub>±.61</sub>	2.31 <sub>±.74</sub>	1.19 <sub>±.15</sub>	1.21 <sub>±.16</sub>	1.41 <sub>±.10</sub>	1.43 <sub>±.10</sub>	0.73 <sub>±.15</sub>	0.75 <sub>±.16</sub>
CFR	2.80 <sub>±.58</sub>	2.74 <sub>±.60</sub>	0.77 <sub>±.18</sub>	0.80 <sub>±.18</sub>	0.73 <sub>±.04</sub>	0.78 <sub>±.04</sub>	1.05 <sub>±.27</sub>	1.08 <sub>±.28</sub>
GANITE	3.02 <sub>±.76</sub>	3.11 <sub>±.74</sub>	0.55 <sub>±.11</sub>	0.60 <sub>±.13</sub>	1.90 <sub>±.40</sub>	2.40 <sub>±.40</sub>	0.77 <sub>±.20</sub>	0.80 <sub>±.24</sub>

## 5.3 Learning the Full Potential Outcome Distributions

Beyond point estimation, PO-Flow offers two distinct advantages for modeling potential outcomes: (1) it enables individualized sampling from the conditional distribution  $P(Y | X, A)$ , generating a

rich set of plausible outcomes for each individual; and (2) it supports learning the density of any generated outcome, providing deeper insights into predictive uncertainty.

### 5.3.1 Learning potential outcome densities

PO-Flow enables direct computation of potential outcome densities, as shown in Proposition 4.7. To evaluate the learned densities, we compute the KL divergence between the PO-Flow estimate  $p_{\theta, Y|X, A}(\cdot|x, a)$  and the ground-truth density  $p_{\text{true}}(\cdot|x, a)$ . Given that the semi-synthetic datasets assume  $y^{(a)} \sim \mathcal{N}(\mu(a), 1)$ , the individual-level KL is  $\text{KL}(\hat{Y}_X^{(a)} \| Y_X^{(a)}) = \mathbb{E}_{\hat{y} \sim p_{\theta, Y|X, A}} \left[ \log \frac{p_{\theta, Y|X, A}(\hat{y}|x, a)}{\mathcal{N}(\hat{y}; \mu(a), 1)} \right]$ , where  $p_{\theta, Y|X, A}$  is computed via (14).

Table 3: KL divergence of learned potential outcome distributions across datasets. Results are averaged over 10-fold cross-validation.

	ACIC 2016	ACIC 2018	IHDP	IBM
PO-Flow	0.14 $\pm$ .04	0.08 $\pm$ .02	0.09 $\pm$ .03	0.08 $\pm$ .03
GP-ITE	1.73 $\pm$ .34	0.73 $\pm$ .19	1.42 $\pm$ .30	0.68 $\pm$ .17

*Baselines:* A natural baseline with density estimation capability is Gaussian Processes for interventional treatment effects, as used in [3, 26].

*Results:* PO-Flow achieves much lower KL divergence than GP baselines on the ACIC 2018, IHDP, and IBM datasets, indicating more accurate density estimation of potential outcomes.

This property enables PO-Flow to identify most likely potential outcomes based on their log-densities. Table 4 reports the RMSE of POs selected by PO-Flow with the highest log-density, illustrating one application of this property.

Table 4: Root mean squared error (RMSE) of estimated potential outcomes (POs) across different methods on the ACIC 2018, IHDP, and IBM datasets. For PO-Flow, results are based on the most likely PO selected from 100 simulated outcomes using log-density.

	ACIC 2018		IHDP		IBM	
	RMSE <sub>in</sub>	RMSE <sub>out</sub>	RMSE <sub>in</sub>	RMSE <sub>out</sub>	RMSE <sub>in</sub>	RMSE <sub>out</sub>
PO-Flow	0.42 $\pm$ .07	0.54 $\pm$ .10	0.96 $\pm$ .09	1.05 $\pm$ .10	0.84 $\pm$ .06	0.90 $\pm$ .08
DiffPO	0.72 $\pm$ .14	0.79 $\pm$ .16	1.33 $\pm$ .20	1.40 $\pm$ .22	1.82 $\pm$ .38	1.85 $\pm$ .35
INFs	0.69 $\pm$ .16	0.78 $\pm$ .17	1.02 $\pm$ .10	1.20 $\pm$ .12	1.52 $\pm$ .24	1.57 $\pm$ .28
S-learner	0.54 $\pm$ .09	0.57 $\pm$ .11	1.31 $\pm$ .18	1.44 $\pm$ .20	1.01 $\pm$ .17	1.16 $\pm$ .19
T-learner	1.57 $\pm$ .32	1.71 $\pm$ .40	1.45 $\pm$ .25	1.49 $\pm$ .27	1.89 $\pm$ .47	1.96 $\pm$ .50
CEVAE	0.83 $\pm$ .17	0.85 $\pm$ .17	1.18 $\pm$ .15	1.36 $\pm$ .18	0.96 $\pm$ .12	0.98 $\pm$ .12
CFR	0.94 $\pm$ .10	0.98 $\pm$ .12	1.10 $\pm$ .20	1.18 $\pm$ .20	2.09 $\pm$ .45	2.17 $\pm$ .48
GANITE	0.88 $\pm$ .15	0.97 $\pm$ .15	1.60 $\pm$ .36	1.67 $\pm$ .34	2.48 $\pm$ .39	2.59 $\pm$ .47

Compared with the averaged RMSE over all POs generated by PO-Flow in Table 1, selecting the most likely POs based on log-density yields smaller RMSEs, providing more confident and closer estimates.

### 5.3.2 Empirical distribution estimations

*Evaluation Metrics:* To enable comparison of estimated potential outcome distributions across methods, we include empirical distribution estimates for all baselines. These are evaluated using the Wasserstein-1 distance, defined as:  $W_1(p_{\theta, Y|X, A}(y|x, a), p_{Y|X, A}(y|x, a)) = \inf_{\gamma \in \Gamma(p_{\theta, p})} \mathbb{E}_{(\hat{y}, y \sim \gamma)} [\|\hat{y} - y\|_1]$ . The results are shown in Table 5.

Table 5: In-sample and out-of-sample Wasserstein distances across different methods on the ACIC 2016, ACIC 2018, IHDP, and IBM datasets. Results are averaged over 10-fold cross-validation.

	ACIC 2016		ACIC 2018		IHDP		IBM	
	$\hat{W}_1^{\text{in}}$	$\hat{W}_1^{\text{out}}$	$\hat{W}_1^{\text{in}}$	$\hat{W}_1^{\text{out}}$	$\hat{W}_1^{\text{in}}$	$\hat{W}_1^{\text{out}}$	$\hat{W}_1^{\text{in}}$	$\hat{W}_1^{\text{out}}$
PO-Flow	<b>0.36</b> $\pm$ .11	<b>0.42</b> $\pm$ .12	<b>0.05</b> $\pm$ .03	<b>0.12</b> $\pm$ .04	<b>0.30</b> $\pm$ .05	<b>0.41</b> $\pm$ .06	<b>0.33</b> $\pm$ .07	<b>0.44</b> $\pm$ .08
DiffPO	0.47 $\pm$ .17	0.51 $\pm$ .18	<b>0.04</b> $\pm$ .02	<b>0.13</b> $\pm$ .05	0.80 $\pm$ .15	0.88 $\pm$ .17	0.69 $\pm$ .14	0.75 $\pm$ .14
INFs	0.59 $\pm$ .13	0.67 $\pm$ .14	0.08 $\pm$ .03	0.16 $\pm$ .05	0.32 $\pm$ .08	<b>0.40</b> $\pm$ .09	0.36 $\pm$ .08	<b>0.45</b> $\pm$ .09
S-learner	1.01 $\pm$ .13	1.02 $\pm$ .20	0.35 $\pm$ .13	0.49 $\pm$ .20	0.71 $\pm$ .14	0.85 $\pm$ .19	0.46 $\pm$ .11	0.55 $\pm$ .14
T-learner	1.22 $\pm$ .15	1.48 $\pm$ .18	1.04 $\pm$ .13	1.00 $\pm$ .30	0.83 $\pm$ .20	0.92 $\pm$ .28	1.21 $\pm$ .23	1.67 $\pm$ .32
CEVAE	0.62 $\pm$ .17	0.70 $\pm$ .21	0.88 $\pm$ .18	1.02 $\pm$ .23	0.65 $\pm$ .14	0.76 $\pm$ .20	0.38 $\pm$ .07	<b>0.45</b> $\pm$ .07
CFR	0.68 $\pm$ .13	0.73 $\pm$ .15	0.88 $\pm$ .12	0.90 $\pm$ .15	0.50 $\pm$ .17	0.56 $\pm$ .19	0.92 $\pm$ .20	0.93 $\pm$ .21
GANITE	0.74 $\pm$ .20	0.86 $\pm$ .23	0.89 $\pm$ .24	1.18 $\pm$ .25	0.71 $\pm$ .23	0.82 $\pm$ .29	1.09 $\pm$ .27	1.34 $\pm$ .30

Understanding the distribution of potential outcomes (POs) is essential for uncertainty-aware treatment decisions, as outcomes for the same individual may vary substantially across treatments. PO-Flow provides not only point estimates but also full distributional insight, enabling practitioners to assess whether outcomes fall within desired ranges and to evaluate their likelihood (Proposition 4.7).

## 5.4 Counterfactual Outcome Estimation

*Evaluation Metrics:* We assess counterfactual predictions using the RMSE between model-estimated  $\hat{y}_{\text{cf}}^{(1-a)}$  and ground-truth  $y_{\text{cf}}^{(1-a)}$ . Results are in Table 6.

*Baselines:* To our knowledge, very few existing methods are specifically designed for counterfactual outcome prediction conditioned on factuials in general settings—without explicitly modeling structural causal models or relying on temporal information. While methods like CFR include “counterfactual” in name, they target unobserved potential outcomes rather than factual-conditioned ones, though we still include them as valuable baselines. We also adapted DiffPO and GANITE for this task, as detailed in Appendix B.5.

Table 6: Root mean squared error (RMSE) of estimated counterfactual outcomes across different methods on the ACIC 2016, ACIC 2018, IHDP, and IBM datasets. Results are averaged over 10-fold cross-validation.

	ACIC 2016		ACIC 2018		IHDP		IBM	
	RMSE $_{\text{in}}$	RMSE $_{\text{out}}$						
PO-Flow	<b>1.50</b> $\pm$ .15	<b>1.53</b> $\pm$ .17	<b>0.04</b> $\pm$ .01	<b>0.05</b> $\pm$ .02	<b>1.63</b> $\pm$ .09	1.69 $\pm$ .10	<b>0.04</b> $\pm$ .01	<b>0.04</b> $\pm$ .02
DiffPO	1.77 $\pm$ .20	1.78 $\pm$ .20	0.62 $\pm$ .14	0.65 $\pm$ .15	1.81 $\pm$ .22	1.85 $\pm$ .23	0.62 $\pm$ .13	0.64 $\pm$ .16
CFR	3.15 $\pm$ .28	3.38 $\pm$ .30	0.99 $\pm$ .05	1.01 $\pm$ .07	<b>1.63</b> $\pm$ .21	<b>1.65</b> $\pm$ .25	0.86 $\pm$ .18	0.87 $\pm$ .16
GANITE	3.41 $\pm$ .52	3.67 $\pm$ .55	0.68 $\pm$ .13	0.70 $\pm$ .14	2.48 $\pm$ .53	2.72 $\pm$ .59	1.84 $\pm$ .30	2.02 $\pm$ .37

## 5.5 Discussions and Comparisons

*Training efficiency:* PO-Flow exhibits high training efficiency, converging in approximately 300 gradient steps across multiple causal datasets (Appendix D.3), and demonstrates notable advantages in both training and sampling time compared to other baselines (Table 9).

*Density estimation for principled uncertainty quantification:* Our continuous normalizing flow (CNF) backbone enables density learning of potential outcomes, as detailed in Section 5.3.1. This property allows us to generate multiple potential outcomes for each individual and to identify the most likely ones based on their log-densities. The empirical evaluation of this procedure is presented in Table 4.

*Counterfactual:* We take a step further by exploring counterfactual outcomes, enabled by the smooth

PO-Flow mapping that preserves factual information during encoding. Under (A1)–(A3), we include a supporting recovery result for this architecture (Proposition 4.3; Corollary 4.5). It is among the first to explore counterfactual outcomes in the potential outcomes framework without relying on temporal data or explicitly modeling structural causal models.

## 6 Conclusions

We introduced PO-Flow, a continuous normalizing flow framework for modeling potential and counterfactual outcomes in causal inference. PO-Flow provides a unified generative framework for potential outcome prediction, CATE estimation, and general-purpose counterfactual prediction in potential outcomes—without explicitly modeling structural causal models (SCMs) or relying on auxiliary information. To our knowledge, this constitutes one of the earliest attempts to address counterfactual outcome prediction in the potential outcomes literature, a crucial yet underexplored direction.

Theoretically, we include a supporting recovery result for the proposed architecture (Corollary 4.5). Empirically, PO-Flow attains state-of-the-art performance on benchmark datasets across standard causal tasks, while additionally supporting counterfactual outcome prediction and log-density estimation for principled uncertainty quantification. In addition, PO-Flow is both computationally efficient and robust compared to modern baselines. These results highlight PO-Flow as a unified and scalable solution for potential-outcomes-based causal tasks, supporting reliable decision-making in domains such as healthcare.

## Acknowledgment

D.I. acknowledges support from NSF (IIS-2212097), ARL (W911NF-2020-221), and ONR (N00014-23-C-1016). Y.X. acknowledges partial support from NSF DMS-2134037, CMMI-2112533, and the Coca-Cola Foundation. Any opinions, findings, and conclusions or recommendations expressed in this material are those of the authors and do not necessarily reflect the views of the sponsor(s).

## References

- [1] Jason Abrevaya, Yu-Chin Hsu, and Robert P Lieli. Estimating conditional average treatment effects. *Journal of Business & Economic Statistics*, 33(4):485–505, 2015.
- [2] Naoufal Acharki, Ramiro Lugo, Antoine Bertonecello, and Josselin Garnier. Comparison of meta-learners for estimating multi-valued treatment heterogeneous effects. In *International conference on machine learning*, pages 91–132. PMLR, 2023.
- [3] Ahmed M Alaa and Mihaela Van Der Schaar. Bayesian inference of individualized treatment effects using multi-task gaussian processes. *Advances in neural information processing systems*, 30, 2017.
- [4] Michael S Albergo and Eric Vanden-Eijnden. Building normalizing flows with stochastic interpolants. *arXiv preprint arXiv:2209.15571*, 2022.
- [5] Ioana Bica, Ahmed M Alaa, James Jordon, and Mihaela van der Schaar. Estimating counterfactual treatment outcomes over time through adversarially balanced representations. *arXiv preprint arXiv:2002.04083*, 2020.

- [6] Tineke Blom, Stephan Bongers, and Joris M Mooij. Beyond structural causal models: Causal constraints models. In *Uncertainty in Artificial Intelligence*, pages 585–594. PMLR, 2020.
- [7] Stephan Bongers, Patrick Forré, Jonas Peters, and Joris M Mooij. Foundations of structural causal models with cycles and latent variables. *The Annals of Statistics*, 49(5):2885–2915, 2021.
- [8] Patrick Chao, Patrick Blöbaum, and Shiva Prasad Kasiviswanathan. Interventional and counterfactual inference with diffusion models. *arXiv preprint arXiv:2302.00860*, 4:16, 2023.
- [9] Patrick Chao, Patrick Blöbaum, Sapan Patel, and Shiva Prasad Kasiviswanathan. Modeling causal mechanisms with diffusion models for interventional and counterfactual queries. *arXiv preprint arXiv:2302.00860*, 2023.
- [10] Ricky TQ Chen, Yulia Rubanova, Jesse Bettencourt, and David K Duvenaud. Neural ordinary differential equations. *Advances in neural information processing systems*, 31, 2018.
- [11] Sitan Chen, Sinho Chewi, Holden Lee, Yuanzhi Li, Jianfeng Lu, and Adil Salim. The probability flow ode is provably fast. *Advances in Neural Information Processing Systems*, 36:68552–68575, 2023.
- [12] Yuansi Chen and Peter Bühlmann. Domain adaptation under structural causal models. *Journal of Machine Learning Research*, 22(261):1–80, 2021.
- [13] Hugh A Chipman, Edward I George, and Robert E McCulloch. Bart: Bayesian additive regression trees. 2010.
- [14] Alicia Curth and Mihaela Van der Schaar. On inductive biases for heterogeneous treatment effect estimation. *Advances in Neural Information Processing Systems*, 34:15883–15894, 2021.
- [15] Alicia Curth and Mihaela Van der Schaar. Nonparametric estimation of heterogeneous treatment effects: From theory to learning algorithms. In *International Conference on Artificial Intelligence and Statistics*, pages 1810–1818. PMLR, 2021.
- [16] Karim Farid, Simon Schrodi, Max Argus, and Thomas Brox. Latent diffusion counterfactual explanations. *arXiv preprint arXiv:2310.06668*, 2023.
- [17] Stefan Feuerriegel, Dennis Frauen, Valentyn Melnychuk, Jonas Schweisthal, Konstantin Hess, Alicia Curth, Stefan Bauer, Niki Kilbertus, Isaac S Kohane, and Mihaela van der Schaar. Causal machine learning for predicting treatment outcomes. *Nature Medicine*, 30(4):958–968, 2024.
- [18] Riccardo Guidotti. Counterfactual explanations and how to find them: literature review and benchmarking. *Data Mining and Knowledge Discovery*, 38(5):2770–2824, 2024.
- [19] P Richard Hahn, Jared S Murray, and Carlos M Carvalho. Bayesian regression tree models for causal inference: Regularization, confounding, and heterogeneous effects (with discussion). *Bayesian Analysis*, 15(3):965–1056, 2020.
- [20] Jason S Haukoos and Roger J Lewis. The propensity score. *Jama*, 314(15):1637–1638, 2015.
- [21] Jennifer L Hill. Bayesian nonparametric modeling for causal inference. *Journal of Computational and Graphical Statistics*, 20(1):217–240, 2011.
- [22] Keisuke Hirano, Guido W Imbens, and Geert Ridder. Efficient estimation of average treatment effects using the estimated propensity score. *Econometrica*, 71(4):1161–1189, 2003.

- [23] Jonathan Ho, Ajay Jain, and Pieter Abbeel. Denoising diffusion probabilistic models. *Advances in neural information processing systems*, 33:6840–6851, 2020.
- [24] Marc Höfler. Causal inference based on counterfactuals. *BMC medical research methodology*, 5: 1–12, 2005.
- [25] Paul W Holland. Statistics and causal inference. *Journal of the American statistical Association*, 81(396):945–960, 1986.
- [26] Bin Huang, Chen Chen, Jinzhong Liu, and Siva Sivaganisan. Gpmatch: A bayesian causal inference approach using gaussian process covariance function as a matching tool. *Frontiers in Applied Mathematics and Statistics*, 9:1122114, 2023.
- [27] Michael F Hutchinson. A stochastic estimator of the trace of the influence matrix for laplacian smoothing splines. *Communications in Statistics-Simulation and Computation*, 18(3):1059–1076, 1989.
- [28] Guido W Imbens. Nonparametric estimation of average treatment effects under exogeneity: A review. *Review of Economics and statistics*, 86(1):4–29, 2004.
- [29] Adrián Javaloy, Pablo Sánchez-Martín, and Isabel Valera. Causal normalizing flows: from theory to practice. *Advances in Neural Information Processing Systems*, 36:58833–58864, 2023.
- [30] Fredrik Johansson, Uri Shalit, and David Sontag. Learning representations for counterfactual inference. In *International conference on machine learning*, pages 3020–3029. PMLR, 2016.
- [31] Fredrik D Johansson, Uri Shalit, Nathan Kallus, and David Sontag. Generalization bounds and representation learning for estimation of potential outcomes and causal effects. *Journal of Machine Learning Research*, 23(166):1–50, 2022.
- [32] Edward H Kennedy. Towards optimal doubly robust estimation of heterogeneous causal effects. *Electronic Journal of Statistics*, 17(2):3008–3049, 2023.
- [33] Sören R Künnel, Jasjeet S Sekhon, Peter J Bickel, and Bin Yu. Metalearners for estimating heterogeneous treatment effects using machine learning. *Proceedings of the national academy of sciences*, 116(10):4156–4165, 2019.
- [34] Lihua Lei and Emmanuel J Candès. Conformal inference of counterfactuals and individual treatment effects. *Journal of the Royal Statistical Society Series B: Statistical Methodology*, 83(5):911–938, 2021.
- [35] Rui Li, Zach Shahn, Jun Li, Mingyu Lu, Prithwish Chakraborty, Daby Sow, Mohamed Ghalwash, and Li-wei H Lehman. G-net: a deep learning approach to g-computation for counterfactual outcome prediction under dynamic treatment regimes. *arXiv preprint arXiv:2003.10551*, 2020.
- [36] Yaron Lipman, Ricky T. Q. Chen, Heli Ben-Hamu, Maximilian Nickel, and Matt Le. Flow matching for generative modeling. In *International Conference on Learning Representations (ICLR)*, 2023. URL <https://arxiv.org/abs/2210.02747>.
- [37] Roderick J Little and Donald B Rubin. Causal effects in clinical and epidemiological studies via potential outcomes: concepts and analytical approaches. *Annual review of public health*, 21(1):121–145, 2000.

- [38] Christos Louizos, Uri Shalit, Joris M Mooij, David Sontag, Richard Zemel, and Max Welling. Causal effect inference with deep latent-variable models. *Advances in neural information processing systems*, 30, 2017.
- [39] Yuchen Ma, Valentyn Melnychuk, Jonas Schweisthal, and Stefan Feuerriegel. Diffpo: A causal diffusion model for learning distributions of potential outcomes. In *Advances in Neural Information Processing Systems (NeurIPS)*, 2024.
- [40] Valentyn Melnychuk, Dennis Frauen, and Stefan Feuerriegel. Causal transformer for estimating counterfactual outcomes. In *International conference on machine learning*, pages 15293–15329. PMLR, 2022.
- [41] Valentyn Melnychuk, Dennis Frauen, and Stefan Feuerriegel. Normalizing flows for interventional density estimation. In *International Conference on Machine Learning*, pages 24361–24397. PMLR, 2023.
- [42] Joris M Mooij, Dominik Janzing, and Bernhard Schölkopf. From ordinary differential equations to structural causal models: the deterministic case. *arXiv preprint arXiv:1304.7920*, 2013.
- [43] Arash Nasr-Esfahany, Mohammad Alizadeh, and Devavrat Shah. Counterfactual identifiability of bijective causal models. In *International conference on machine learning*, pages 25733–25754. PMLR, 2023.
- [44] Leland Gerson Neuberger. Causality: models, reasoning, and inference, by judea pearl, cambridge university press, 2000. *Econometric Theory*, 19(4):675–685, 2003.
- [45] Nick Pawlowski, Daniel Coelho de Castro, and Ben Glocker. Deep structural causal models for tractable counterfactual inference. *Advances in neural information processing systems*, 33: 857–869, 2020.
- [46] Mattia Prospero, Yi Guo, Matt Sperrin, James S Koopman, Jae S Min, Xing He, Shannan Rich, Mo Wang, Iain E Buchan, and Jiang Bian. Causal inference and counterfactual prediction in machine learning for actionable healthcare. *Nature Machine Intelligence*, 2(7):369–375, 2020.
- [47] Donald B Rubin. Causal inference using potential outcomes: Design, modeling, decisions. *Journal of the American statistical Association*, 100(469):322–331, 2005.
- [48] Pedro Sanchez and Sotirios A Tsaftaris. Diffusion causal models for counterfactual estimation. *arXiv preprint arXiv:2202.10166*, 2022.
- [49] Jonas Schweisthal, Dennis Frauen, Mihaela Van Der Schaar, and Stefan Feuerriegel. Meta-learners for partially-identified treatment effects across multiple environments. In *Forty-first International Conference on Machine Learning*, 2024.
- [50] Uri Shalit, Fredrik D Johansson, and David Sontag. Estimating individual treatment effect: generalization bounds and algorithms. In *International conference on machine learning*, pages 3076–3085. PMLR, 2017.
- [51] Yishai Shimoni, Chen Yanover, Ehud Karavani, and Yaara Goldschmndt. Benchmarking framework for performance-evaluation of causal inference analysis. *arXiv preprint arXiv:1802.05046*, 2018.

- [52] Jiaming Song, Chenlin Meng, and Stefano Ermon. Denoising diffusion implicit models. *arXiv preprint arXiv:2010.02502*, 2020.
- [53] Yang Song, Jascha Sohl-Dickstein, Diederik P Kingma, Abhishek Kumar, Stefano Ermon, and Ben Poole. Score-based generative modeling through stochastic differential equations. *arXiv preprint arXiv:2011.13456*, 2020.
- [54] Yang Song, Prafulla Dhariwal, Mark Chen, and Ilya Sutskever. Consistency models. 2023.
- [55] Eric V Strobl and Thomas A Lasko. Identifying patient-specific root causes with the heteroscedastic noise model. *Journal of Computational Science*, 72:102099, 2023.
- [56] Marc K Walton, John H Powers III, Jeremy Hobart, Donald Patrick, Patrick Marquis, Spiros Vamvakas, Maria Isaac, Elizabeth Molsen, Stefan Cano, and Laurie B Burke. Clinical outcome assessments: conceptual foundation—report of the ispor clinical outcomes assessment—emerging good practices for outcomes research task force. *Value in Health*, 18(6):741–752, 2015.
- [57] Shenghao Wu, Wenbin Zhou, Minshuo Chen, and Shixiang Zhu. Counterfactual generative models for time-varying treatments. In *Proceedings of the 30th ACM SIGKDD Conference on Knowledge Discovery and Data Mining*, pages 3402–3413, 2024.
- [58] Chen Xu, Xiuyuan Cheng, and Yao Xie. Normalizing flow neural networks by jko scheme. *Advances in Neural Information Processing Systems*, 36:47379–47405, 2023.
- [59] Mengyue Yang, Furui Liu, Zhitang Chen, Xinwei Shen, Jianye Hao, and Jun Wang. Causalvae: Disentangled representation learning via neural structural causal models. In *Proceedings of the IEEE/CVF conference on computer vision and pattern recognition*, pages 9593–9602, 2021.
- [60] Zhen Yang, Yongbin Liu, Chunping Ouyang, Lin Ren, and Wen Wen. Counterfactual can be strong in medical question and answering. *Information Processing & Management*, 60(4):103408, 2023.
- [61] Jinsung Yoon, James Jordon, and Mihaela Van Der Schaar. Ganite: Estimation of individualized treatment effects using generative adversarial nets. In *International conference on learning representations*, 2018.
- [62] Kun Zhang and Aapo Hyvarinen. On the identifiability of the post-nonlinear causal model. *arXiv preprint arXiv:1205.2599*, 2012.
- [63] Zhiwei Zhang, Chenguang Wang, Lei Nie, and Guoxing Soon. Assessing the heterogeneity of treatment effects via potential outcomes of individual patients. *Journal of the Royal Statistical Society Series C: Applied Statistics*, 62(5):687–704, 2013.
- [64] Zeyu Zhou, Ruqi Bai, Sean Kulinski, Murat Kocaoglu, and David I Inouye. Towards characterizing domain counterfactuals for invertible latent causal models. *arXiv preprint arXiv:2306.11281*, 2023.

## A Proofs

**Proposition A.1.** *Assume that  $p(y|x, a) > 0$  for all  $y$  and  $t \in [0, 1]$ . Then, up to a constant independent of  $\theta$ , the Conditional Flow Matching (CFM) loss and the original Flow Matching (FM) loss are equivalent. Hence,*

$$\nabla_{\theta} \mathcal{L}_{FM}(\theta) = \nabla_{\theta} \mathcal{L}_{CFM}(\theta).$$

*Proof:*

We denote the conditional reference velocity field as  $u(y, t, x, a|y_0) = \frac{d\phi}{dt} = (1 - \sigma_{\min})y_1 - y_0$ , as defined in (6). We further define the marginal (unconditional) reference velocity field as:

$$u(y, t, x, a) = \int u(y, t, x, a|y_0) \frac{p(y, t, x, a|y_0)p_Y(y_0)}{p(y, t, x, a)} dy_0, \quad (15)$$

where  $p(y, t, x, a|y_0)$  and  $p(y, t, x, a)$  denote the probability densities induced by  $u(y, t, x, a|y_0)$  and  $u(y, t, x, a)$ , respectively. Next, the original flow matching loss, unconditioned on  $y_0$ , is defined as:

$$\mathcal{L}_{FM} = \mathbb{E}_{t \sim \mathcal{U}[0,1], p_{Y,X,A}(\cdot)} \|v_{\theta}(y, t, x, a) - u(y, t, x, a)\|^2. \quad (16)$$

In the main text, we chose  $\phi$  as the linear interpolant between  $y_0$  and  $y_1$ , which results in a constant reference velocity  $\frac{d\phi}{dt}$  independent of  $t$ . This leads to the simplified CFM loss presented in Eq. (9). However, the general CFM loss, corresponding to an arbitrary reference velocity field  $u(y, t | y_0)$  conditioned on  $y_0$ , is defined as:

$$\mathcal{L}_{CFM} = \mathbb{E}_{t \sim \mathcal{U}[0,1], p_Y(y_0), p_{Y,X,A|Y_0}(\cdot|y_0)} \|v_{\theta}(\cdot) - u(\cdot|y_0)\|^2 \quad (17)$$

Next, we have that:

$$\begin{aligned} \|v_{\theta}(y, t, x, a) - u(y, t, x, a)\|^2 &= \|v_{\theta}(\cdot)\|^2 - 2\langle v_{\theta}(\cdot), u(\cdot) \rangle + \|u(\cdot)\|^2 \\ \|v_{\theta}(y, t, x, a) - u(y, t, x, a|y_0)\|^2 &= \|v_{\theta}(\cdot)\|^2 - 2\langle v_{\theta}(\cdot), u(\cdot|y_0) \rangle + \|u(\cdot|y_0)\|^2. \end{aligned} \quad (18)$$

Besides, the term  $\mathbb{E}_{t \sim \mathcal{U}[0,1], p_{Y,X,A}(\cdot)} \|v_{\theta}(\cdot)\|^2$  can be equivalently expressed in conditional form as:

$$\begin{aligned} \mathbb{E}_{t \sim \mathcal{U}[0,1], p_{Y,X,A}(\cdot)} \|v_{\theta}(\cdot)\|^2 &= \int \|v_{\theta}(\cdot)\|^2 p_{Y,X,A}(\cdot) dy dx da dt \\ &= \int \|v_{\theta}(\cdot)\|^2 p_{Y,X,A|Y_0}(\cdot|y_0) p_Y(y_0) dy_0 dy dx da dt \\ &= \mathbb{E}_{t \sim \mathcal{U}[0,1], p_Y(y_0), p_{Y,X,A|Y_0}(\cdot|y_0)} \|v_{\theta}(\cdot)\|^2. \end{aligned} \quad (19)$$

Furthermore, by the law of total expectation, we have:

$$\begin{aligned} \mathbb{E}_{t \sim \mathcal{U}[0,1], p_{Y,X,A}(\cdot)} \langle v_{\theta}(\cdot), u(\cdot) \rangle &= \int \left\langle v_{\theta}(\cdot), \frac{\int u(\cdot|y_0) p_{Y,X,A}(\cdot|y_0) p_Y(y_0) dy_0}{p_{Y,X,A}(\cdot)} \right\rangle p_{Y,X,A}(\cdot) dy dx da dt \\ &= \int \left\langle v_{\theta}(\cdot), \int u(\cdot|y_0) p_{Y,X,A}(\cdot|y_0) p_Y(y_0) dy_0 \right\rangle dy dx da dt \\ &= \int \langle v_{\theta}(\cdot), u(\cdot|y_0) \rangle p_{Y,X,A}(\cdot|y_0) p_Y(y_0) dy_0 dy dx da dt \\ &= \mathbb{E}_{t \sim \mathcal{U}[0,1], p_Y(y_0), p_{Y,X,A|Y_0}(\cdot|y_0)} \langle v_{\theta}(\cdot), u(\cdot|y_0) \rangle. \end{aligned} \quad (20)$$

Finally, because  $u(\cdot | y_0)$  does not depend on  $\theta$ , substituting Eqs. (19) and (20) into Eq. (16) and differentiating with respect to  $\theta$  yields:

$$\nabla_{\theta} \mathcal{L}_{\text{FM}}(\theta) = \nabla_{\theta} \mathcal{L}_{\text{CFM}}(\theta). \quad (21)$$

**Proposition 4.3.** (Encoded  $Z$  as a function of the exogenous noise  $U$ ) *Let Assumption 4.1 hold. Assume that the exogenous noise  $U \sim \text{Unif}[0, 1]$ . Then there exists a continuously differentiable bijection function  $\psi_X : \mathcal{U} \rightarrow \mathcal{Z}$  that is independent of the treatment assignment  $A$ , i.e.,*

$$Z = \Phi_{\theta}(Y^{(A)}; X, A) = \Phi_{\theta}(f_X(A, U); X, A) = \psi_X(U) \quad \text{a.s.} \quad (22)$$

*Proof.* Based on the structural causal model, we have  $Y^{(A)} = f_X(A, U)$ . We define

$$m_{X,A}(U) := Z = \Phi_{\theta}(Y^{(A)}; X, A) = \Phi_{\theta}(f_X(A, U); X, A),$$

as a function that may depend on the action  $A$ . Therefore, our target becomes proving that  $m_{X,A}(U)$  is functionally invariant to  $A$ .

By (A3) in Assumption 4.1, we have  $Z \perp\!\!\!\perp A | X$ . Therefore,

$$p_{\theta, Z|X,A}(z) = p_{\theta, Z}(z). \quad (23)$$

In continuous normalizing flows,  $\Phi_{\theta}$  is invertible with respect to  $Y^{(A)}$  due to the invertibility of the underlying neural ODE. In 1-D, this implies that  $\Phi_{\theta}$  is monotonic in  $Y^{(A)} = f_X(A, U)$ . Without loss of generality, we assume that  $\Phi_{\theta}$  is strictly increasing in  $f_X$ .

Moreover, by (A2), since  $f_X(\cdot, U)$  is strictly monotone in  $U$ . Without loss of generality, we assume strictly increasing. Then it follows by the composition rule that  $m_{X,A}(U)$  is strictly increasing in  $U$  and hence bijective on  $[0, 1]$ .

Since  $Z = \Phi_{\theta}(Y^{(A)}; X, A) = m_{X,A}(U)$ , we may apply change of variables formula w.r.t.  $U$ :

$$p_{\theta, Z|X,A}(z) = p_U(m_{X,A}^{-1}(z)) \left| \frac{d}{dz} m_{X,A}^{-1}(z) \right| = 1 \cdot \frac{d}{dz} m_{X,A}^{-1}(z), \quad (24)$$

where the last equation follows from the uniform distribution of  $U$  and the fact that  $p_Z > 0$ .

Then based on (23), we have:

$$p_{\theta, Z|X,A=1}(z) = \frac{d}{dz} m_{X,1}^{-1}(z) = \frac{d}{dz} m_{X,0}^{-1}(z) = p_{\theta, Z|X,A=0}(z). \quad (25)$$

It follows that:

$$m_{X,A}^{-1}(z) = \int^z \frac{d}{dt} m_{X,A}^{-1}(t) dt = \int^z c(t) dt + c_A, \quad (26)$$

where  $c(t) = \frac{d}{dt} m_{X,1}^{-1}(t) = \frac{d}{dt} m_{X,0}^{-1}(t)$  is independent of  $A$ , and  $c_A$  is a constant for each  $A$ .

By re-inverting (26), we have:

$$m_{X,A}(u) = (m_{X,A}^{-1})^{-1}(u) = \left( \underbrace{\int^{\bullet} c(t) dt + c_A}_{:=H(\bullet)} \right)^{-1}(u) = H^{-1}(u - c_A). \quad (27)$$

Since  $m_{X,A}$  is a bijection  $[0, 1] \rightarrow \text{supp}(Z) = \{z \in \mathbb{R} : p_Z(z) > 0\}$ , we have:

$$m_{X,A}(0) = \inf \text{supp}(Z), \quad m_{X,A}(1) = \sup \text{supp}(Z), \quad \text{for both } A. \quad (28)$$

Besides, since the support of  $Z$  does not depend on  $A$  because of (23), we have that

$$\inf \text{supp}(Z) = m_{X,0}(0) = H^{-1}(-c_0) = H^{-1}(-c_1) = m_{X,1}(0). \quad (29)$$

Therefore,  $c_0 = c_1 := c$  is a constant that does not depend on  $A$ .

Therefore, we can write

$$\psi_X(U) := H^{-1}(U - c) = m_{X,0}(U) = m_{X,1}(U). \quad (30)$$

As a result, we conclude that

$$Z = \Phi_\theta(Y^{(A)}; X, A) = \psi_X(U) \quad \text{a.s.}, \quad (31)$$

is a function that only depends on the exogenous noise  $U$  (and covariates  $X$ ), and is invariant to the treatment  $A$ .

**Corollary 4.5** (Counterfactual recovery) *Assume the conditions in Assumption 4.1 hold. Consider a factual sample  $(Y^{(A)}, X, A)$  given by the structural equation  $Y^{(A)} = f_X(A, U)$ , and let its encoded representation be  $Z = \Phi_\theta(Y^{(A)}; X, A)$ . Apply the intervention  $\text{do}(A = \gamma)$ . Assume that the true counterfactual is given by  $Y_{\text{CF}}^{(\gamma)} = f_X(\gamma, U)$ .*

*The decoder then recovers the counterfactual almost surely:*

$$\hat{Y}_{\text{CF}}^\gamma := \Phi_\theta^{-1}(Z; X, \gamma) = Y_{\text{CF}}^\gamma. \quad (32)$$

*Proof.* Due to the deterministic and invertible nature of the continuous normalizing flow when the conditioning input is fixed, we have,

$$\Phi_\theta^{-1}(\Phi_\theta(Y; X, A); X, A) = Y. \quad (33)$$

From Proposition 4.3, we have  $Z = \Phi_\theta(Y^{(A)}; X, A) = \Phi_\theta(f_X(A, U); X, A) = \psi_X(U)$  does not depend on  $A$ . Therefore, fixing  $U$  as the same and plugging in  $\text{do}(A = \gamma)$ , we have:

$$\Phi_\theta(Y^{(A)}; X, A) = \Phi_\theta(f_X(A, U); X, A) = \psi_X(U) = \Phi_\theta(f_X(\gamma, U); X, \gamma) = \Phi_\theta(Y_{\text{CF}}^\gamma; X, \gamma), \quad (34)$$

or more simply,

$$\Phi_\theta(Y^{(A)}; X, A) = \Phi_\theta(Y_{\text{CF}}^\gamma; X, \gamma), \quad (35)$$

we further have,

$$\Phi_\theta^{-1}(\Phi_\theta(Y^{(A)}; X, A); X, \gamma) = \Phi_\theta^{-1}(\Phi_\theta(Y_{\text{CF}}^\gamma; X, \gamma); X, \gamma). \quad (36)$$

Noting that the L.H.S. of (36) is exactly the counterfactual procedures (encoding-decoding) of PO-Flow, and by (33), the R.H.S. of (36) equals to  $Y_{\text{CF}}^\gamma$ . Therefore,

$$\hat{Y}_{\text{CF}}^\gamma := \Phi_\theta^{-1}(Z; X, \gamma) = Y_{\text{CF}}^\gamma. \quad (37)$$

**Proposition 4.7.** *Given a noise sample  $z \sim q(\cdot)$  at  $t = 1$ , the log-density of the resulting potential outcome at  $t = 0$ , obtained via PO-Flow, is given by:*

$$\log p_{\theta, Y|X, A}(y(0) | x, a, z) = \log q(z) + \int_0^1 \nabla_y \cdot v_{\theta}(y(t), t; x, a) dt.$$

*Proof:*

Samples from Continuous Normalizing Flows (CNFs) evolve according to the following Neural ODE:

$$\frac{dy(t)}{dt} = v_{\theta}(y(t), t; x, a), \quad t \in [0, 1], \quad (38)$$

which induces a corresponding evolution of the sample density governed by the Liouville continuity equation:

$$\partial_t p_{\theta}(y, t) + \nabla \cdot (p_{\theta}(y, t) v_{\theta}(y, t; x, a)) = 0. \quad (39)$$

Here,  $p_{\theta}(y, t)$  denotes the time-dependent probability density of the samples  $y$ .

Next, we have that the dynamics of the density  $p_{\theta}(\cdot)$  governed by the velocity field  $v_{\theta}(y, t, x, a)$  is given by:

$$\frac{d}{dt} \log p_{\theta}(y(t), t) = \frac{\nabla p_{\theta}(y(t), t) \cdot \partial_t y(t) + \partial_t p_{\theta}(y(t), t)}{p_{\theta}(y(t), t)} \quad (40)$$

$$= \frac{\nabla p_{\theta} \cdot \partial_t y + \partial_t p_{\theta}}{p_{\theta}} \Big|_{(y(t), t)} \quad (41)$$

$$= \frac{\nabla p_{\theta} \cdot v_{\theta} - \nabla \cdot (p_{\theta} v_{\theta})}{p_{\theta}} \Big|_{(y(t), t)} \quad (\text{by (38) and (39)}) \quad (42)$$

$$= \frac{\nabla p_{\theta} \cdot v_{\theta} - (\nabla p_{\theta} \cdot v_{\theta} + p_{\theta} \nabla \cdot v_{\theta})}{p_{\theta}} \Big|_{(y(t), t)} \quad (43)$$

$$= -\nabla \cdot v_{\theta}. \quad (44)$$

Starting from an initial sample  $z \sim q(\cdot)$  and integrating from  $t = 1$  to  $t = 0$ , we have:

$$\log p_{\theta, Y|X, A}(y(0) | x, a, z) = \log q(z) + \int_0^1 \nabla_y \cdot v_{\theta}(y(t), t; x, a) dt. \quad (45)$$

Besides, if  $q(\cdot)$  is selected as the commonly used  $N(0, I)$ , we have:

$$\log p_{\theta, Y|X, A}(y(0) | x, a, z) = -\frac{d_Y}{2} \log 2\pi - \frac{1}{2} \|z\|^2 + \int_0^1 \nabla_y \cdot v_{\theta}(y(t), t; x, a) dt. \quad (46)$$

## B Experimental Details

### B.1 Synthetic Causal Datasets

Counterfactual outcomes are unobservable in real-world data but can be simulated using synthetic datasets. In our experiments, we evaluate on widely used benchmarks, including the Atlantic Causal

Inference Conference datasets (ACIC 2016 and ACIC 2018), the Infant Health and Development Program (IHDP) [21, 38], and the IBM Causal Inference Benchmark [51].

The ACIC 2016 dataset contains 4,802 samples with 82 covariates each ( $d_X = 82$ ), ACIC 2018 has 1,000 samples with 177 covariates, IHDP includes 747 samples with 25 covariates, and the IBM dataset consists of 1,000 samples with 177 covariates. Each dataset provides three synthetic values per individual: the factual outcome  $y^{(a)}$ , the assigned treatment  $a$ , and the mean potential outcomes under both treatments,  $\mu_0$  (for  $a = 0$ ) and  $\mu_1$  (for  $a = 1$ ).

Moreover, under the following dataset synthesis assumptions: (1) fully specified outcome model  $Y^{(A)} = f(X, A) + \epsilon$ ; (2) shared noise across treatment arms for each individual; and (3) invertibility of the structural function such that, given  $X$ ,  $A$ , and  $Y^{(A)}$ , one can solve for  $\epsilon$  — we can synthesize the counterfactual outcome through the following procedure:

1. **Abduction:** infer the unobserved noise term  $\epsilon'$  from the factual outcome  $Y^{(A)}$ , covariates  $X$ , and treatment  $A$ ;
2. **Action:** intervene by changing the treatment assignment to  $1 - A$ ;
3. **Prediction:** use the inferred noise  $\epsilon'$  and new treatment to compute the counterfactual outcome via  $Y^{(1-A)} = f(X, 1 - A) + \epsilon'$ .

All datasets are generated using diverse simulation mechanisms, and we provide the specific versions used along with our code. For example, the IHDP dataset is generated using 25 covariates and a coefficient matrix  $W$ , following the data-generating process:

$$\begin{aligned}
 X &\sim \text{Real-world distribution } p_X(\cdot), \\
 A &\sim \text{Real-world Treatment assignment based on } X, \\
 Y &= A(X\beta - \omega) + (1 - A)\exp((X + W)\beta) + \epsilon, \quad \epsilon \sim N(0, 1).
 \end{aligned}
 \tag{47}$$

where  $\beta$ ,  $W$ , and  $\omega$  are parameters defined by the specific simulation setting.

## B.2 Neural Network Structure and Implementation Information

The neural network used in experiments on causal datasets takes as input  $y(t)$ ,  $x$ ,  $t$ , and  $a$ . The model is composed of the following components: (1) an outcome embedding layer that projects  $y(t)$  to the same dimension as the concatenated  $(x, a)$ ; (2) a FiLM layer that applies feature-wise affine transformations to the embedded  $y(t)$ , conditioned on  $(x, a)$ ; (3) two residual blocks, each consisting of a gated two-layer MLP conditioned on  $(x, a)$ , with residual averaging and skip connections; and (4) a projection layer that maps the final hidden representation to two velocity vectors  $v_0$  and  $v_1$ , corresponding to treatments 0 and 1.

All experiments are conducted on an A100 GPU with 16 GB of memory. The training time for causal datasets depends on the dataset and batch sizes. For example, training on the ACIC 2018 dataset with a batch size of 256 typically takes 2–4 seconds per epoch. Log-density evaluation, as discussed in Section 4.3, involves divergence integration and requires significantly more time than other test metrics.

### B.3 Runge-Kutta numerical integration method

We apply the classical 4th-order Runge-Kutta method to solve the Neural ODE in the forward process of PO-Flow. Given a factual outcome  $y^{(a)}$ , we aim to compute the latent embedding  $z = y(1)$  by integrating the velocity field  $v_\theta$  from  $t = 0$  to  $t = 1$ , with initial condition  $y(0) = y^{(a)}$ . Let  $h$  denote the step size, and define discrete time steps  $t_k = kh$ , for  $k = 0, 1, \dots, T$ , such that  $Th = 1$ . The update rule at each step is:

$$y(t_{k+1}) = y(t_k) + \frac{h}{6} (k_1 + 2k_2 + 2k_3 + k_4),$$

where

$$\begin{aligned} k_1 &= v_\theta(y(t_k), t_k, x, a), \quad k_2 = v_\theta\left(y(t_k) + \frac{h}{2}k_1, t_k + \frac{h}{2}, x, a\right), \\ k_3 &= v_\theta\left(y(t_k) + \frac{h}{2}k_2, t_k + \frac{h}{2}, x, a\right), \quad k_4 = v_\theta(y(t_k) + hk_3, t_k + h, x, a), \end{aligned}$$

with  $y(0) = y^{(a)}$  and  $y(1) = z$ . This produces a numerically integrated trajectory from the observed sample to its latent representation.

### B.4 Hutchinson trace estimator

The computations of the log-density of the POs involve the calculation of  $\nabla \cdot v_k(x, t)$ , i.e., the divergence of the velocity field represented by a neural network. This may be computed by brute force using reverse-mode automatic differentiation, which is much slower and less stable in high dimensions.

We can express  $\nabla \cdot v_\theta(y, t, x, a) = \mathbb{E}_{\epsilon \sim p(\epsilon)} [\epsilon^T J_v(y)\epsilon]$ , where  $J_v(y)$  is the Jacobian of  $v_\theta(y, t, x, a)$  at  $y$ . Given a fixed  $\epsilon$ , we have  $J_v(y)\epsilon = \lim_{\sigma \rightarrow 0} \frac{v_\theta(y + \sigma\epsilon, t, x, a) - v_\theta(y, t, x, a)}{\sigma}$ , which is the directional derivative of  $v_\theta$  along the direction  $\epsilon$ . Therefore, for a sufficiently small  $\sigma > 0$ , we can propose the following Hutchinson estimator [27, 58]:

$$\nabla \cdot v_\theta(y(t), t, x, a) \approx \mathbb{E}_{p(\epsilon)} \left[ \epsilon \cdot \frac{v_\theta(y(t) + \sigma\epsilon, t, x, a) - v_\theta(y(t), t, x, a)}{\sigma} \right], \quad (48)$$

where  $p(\epsilon)$  is a distribution in  $\mathbb{R}^{d_Y}$  satisfying  $\mathbb{E}[\epsilon] = 0$  and  $\text{Cov}(\epsilon) = I$  (e.g., a standard Gaussian). This approximation becomes exact as  $\sigma \rightarrow 0$ .

### B.5 Adapted Implementation Details for DiffPO and GANITE Counterfactuals

DiffPO was not originally designed for counterfactual tasks. However, since DiffPO uses a diffusion model as its base, we are able to adapt the algorithm to incorporate an "encoding" and "decoding" structure similar to that of PO-Flow. Our adapted implementation of their algorithm for counterfactual estimation is summarized in Algorithm 3.

---

**Algorithm 3:** Adapted DiffPO for Counterfactual
 

---

- Input:**  $(y^{(a)}, x, a) \sim p_{Y,X,A}(\cdot)$
- 1:  $z_0 \leftarrow y^{(a)}$
  - 2: Forward Process:
  - 3: for  $t = 0, \dots, T - 1$ :
  - 4:  $z_{t+1} \leftarrow \sqrt{\frac{\alpha_{t+1}}{\alpha}} z + f_{\theta}(z, t|x, a) \left( \sqrt{1 - \alpha_{t+1}} - \sqrt{\frac{\alpha_{t+1}(1-\alpha)}{\alpha}} \right)$
  - 5:  $z \leftarrow z_T$
  - 6: Reverse Process:
  - 7: Follow their official implementation in Section 5.3
  - 8: **Return**  $\hat{y}^{(1-a)} := \hat{y}_0$
- 

Similarly, GANITE was not originally designed for counterfactual inference. It consists of a generator and a discriminator, with the final output targeting CATE estimation. However, the generator also produces a proxy counterfactual given the factual input, which we use to evaluate its counterfactual estimation performance.

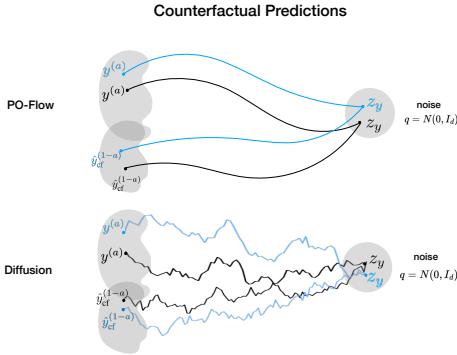


Figure 2: Illustration of counterfactual predictions. *Left:* two potential outcomes distribution. *Right:* Base (noise) distribution.

As shown in Figure 2, standard diffusion models use noisy and stochastic forward processes that may degrade the information in  $z$ , producing reverse samples that resemble interventional potential outcomes rather than counterfactuals.

In practice, probability flow ODEs [53, 11] or DDIM [52] can be applied to obtain a velocity field equivalent to the ODE derived from the trained diffusion score/noise, under which diffusion and flow matching are theoretically equivalent.

## C Comparisons to BGM settings

**Bijection Generation Mechanisms (BGM).** The BGM framework [43] shows that if the true structural mechanism  $f$  is in the BGM class (bijective/strictly monotone in the exogenous noise), then any learned mechanism  $\hat{f}$  that (i) is also in the BGM class and (ii) *matches the observed distribution*—i.e., for the same parents value  $X$  and action  $A$ ,

$$\hat{f}_X(A, U) \stackrel{d}{=} f_X(A, U) \quad (\text{equivalently } (\hat{f}(X, \cdot))_{\#} P_U = (f(X, \cdot))_{\#} P_U),$$

yields the *same counterfactuals* as  $f$ . Their result is model-agnostic, at the class level.

**PO-Flow.** Our findings are specific to a particular methodology and architecture, as this is a methodology paper where we analyze continuous normalizing flows (CNFs). With the additional assumption (A3) specific to PO-Flow, Proposition 4.3 shows that the PO-Flow encoded latent  $Z$

is bijective in the exogenous noise  $U$ . Consequently, Corollary 4.5 proves that the encode–decode procedure recovers the true counterfactual.

**Relationships.** Because of Proposition 4.3 (enabled by the CNF), PO-Flow implements a bijective-in-noise mechanism and is thus comparable to BGM in the sense that  $\hat{f}$  is bijective in  $U$ . However, BGM additionally requires observational distribution matching to obtain class-level identifiability, whereas the proofs of Proposition 4.3 and Corollary 4.5 do not assume such matching.

**Alternative route.** The counterfactual recovery result (Corollary 4.5) can alternatively be established by imposing an additional assumption:

**(A4) Observational matching.** For each  $(x, a)$ , the PO-Flow–induced observational law matches the true one, i.e.,

$$(\hat{f}_X(a, \cdot))_{\#} P_U = (f_X(a, \cdot))_{\#} P_U.$$

Under (A1)–(A3), Proposition 4.3 establishes a continuously differentiable bijection  $\psi_X : U \rightarrow Z$  (independent of  $A$ ), so the induced mechanism  $\hat{f}_X$  implemented by PO-Flow is bijective in the exogenous noise, i.e., PO-Flow lies in the BGM class. With the additional assumption (A4), we can therefore directly invoke the counterfactual recovery result of the BGM framework [43].

## D Additional Experimental Results

### D.1 Empirical Validation of Assumption (A3)

We test (A3):  $p_\theta(Z | X, A) = q(Z) = \mathcal{N}(0, 1)$ , using a two-sample Maximum Mean Discrepancy (MMD). Specifically, we test the joint factorization  $p(Z, X, A) = q(Z)p(X, A)$  by computing the MMD between the empirical joint sample  $\{(z_i, x_i, a_i)\}$  and a synthetic joint sample  $\{(z'_i, x_i, a_i)\}$ , where  $z'_i \sim q = \mathcal{N}(0, 1)$ .

We employ a product kernel  $k((z, x, a), (z', x', a')) = k_Z(z, z') \cdot k_X(x, x') \cdot k_A(a, a')$ , where  $k_Z(z, z')$  and  $k_X(x, x')$  are radial basis function (RBF) mixtures and  $k_A(a, a') = \mathbf{1}[a = a']$  is the indicator kernel for discrete actions:

$$\begin{aligned} k_Z(z, z') &= \exp\left(-\frac{\|z - z'\|^2}{2\sigma_Z^2}\right), \\ k_X(x, x') &= \exp\left(-\frac{\|x - x'\|^2}{2\sigma_X^2}\right). \end{aligned} \tag{49}$$

To set the bandwidths  $\{\sigma_Z\}$  and  $\{\sigma_X\}$ , we first compute the pooled pairwise distances on the union of the observed and synthetic sets (e.g.,  $\tilde{Z} = Z \cup Z'$ ). We then calculate the median of these distances, and define the bandwidths as  $\frac{1}{2}$  median. The empirical MMD is given as:

$$\widehat{\text{MMD}}_u^2 = \frac{1}{n(n-1)} \sum_{i \neq j} k(u_i, u_j) + \frac{1}{n(n-1)} \sum_{i \neq j} k(v_i, v_j) - \frac{2}{n(n-1)} \sum_{i \neq j} k(u_i, v_j), \tag{50}$$

with  $u_i = (z_i, x_i, a_i)$ ,  $v_i = (z'_i, x_i, a_i)$ .

For more reliable comparisons, we additionally sample two ground-truth sets,  $\{(z'_i, x_i, a_i)\}$  and  $\{(z''_i, x_i, a_i)\}$ , where both  $z'_i \sim \mathcal{N}(0, 1)$  and  $z''_i \sim \mathcal{N}(0, 1)$ . The test is conducted on each dataset considered in the paper, and the aggregated results are summarized in the table below.

Table 7: Empirical validation of Assumption (A3),  $p_\theta(Z | X, A) = q(Z) = \mathcal{N}(0, 1)$ . We report two-sample MMD values comparing the empirical joint distribution  $\{(z_i, x_i, a_i)\}$  with synthetic samples  $\{(z'_i, x_i, a_i)\}$  across datasets. Lower MMD indicates closer agreement with the assumed factorization  $p(Z, X, A) = q(Z)p(X, A)$ .

	ACIC 2016	ACIC 2018	IHDP	IBM
<b>PO-Flow</b>	$4.9 \times 10^{-2}$	$7.2 \times 10^{-3}$	$2.7 \times 10^{-2}$	$6.8 \times 10^{-2}$
True	$4.1 \times 10^{-2}$	$5.9 \times 10^{-3}$	$2.5 \times 10^{-2}$	$5.3 \times 10^{-2}$

As shown in Table 7, PO-Flow achieves small two-sample joint MMD values, which are comparable to those obtained from the ground-truth independent samples  $\{(z'_i, x_i, a_i)\}$  and  $\{(z''_i, x_i, a_i)\}$ . This provides empirical support for the validity of Assumption (A3).

## D.2 Identifying the Most Likely Potential Outcomes via Log-Density

As shown in Proposition 4.7 and Section 5.3.1, we can naturally select the most likely potential outcome based on log-density. Table 8 reports the RMSE of PO-Flow when using the most likely PO selected by the algorithm. Specifically, for each sample we simulate 100 POs with PO-Flow, select the one with the highest log-density, and compute the results accordingly.

Table 8: Root mean squared error (RMSE) of estimated potential outcomes (POs) across different methods on the ACIC 2018, IHDP, and IBM datasets. For PO-Flow, results are based on the most likely PO selected from 100 simulated outcomes using log-density. All values are averaged over 10-fold cross-validation.

	ACIC 2018		IHDP		IBM	
	RMSE <sub>in</sub>	RMSE <sub>out</sub>	RMSE <sub>in</sub>	RMSE <sub>out</sub>	RMSE <sub>in</sub>	RMSE <sub>out</sub>
<b>PO-Flow</b>	<b>0.42<math>\pm</math>.07</b>	<b>0.54<math>\pm</math>.10</b>	<b>0.96<math>\pm</math>.09</b>	<b>1.05<math>\pm</math>.10</b>	<b>0.84<math>\pm</math>.06</b>	<b>0.90<math>\pm</math>.08</b>
DiffPO	0.72 $\pm$ .14	0.79 $\pm$ .16	1.33 $\pm$ .20	1.40 $\pm$ .22	1.82 $\pm$ .38	1.85 $\pm$ .35
INFs	0.69 $\pm$ .16	0.78 $\pm$ .17	1.02 $\pm$ .10	1.20 $\pm$ .12	1.52 $\pm$ .24	1.57 $\pm$ .28
S-learner	0.54 $\pm$ .09	0.57 $\pm$ .11	1.31 $\pm$ .18	1.44 $\pm$ .20	1.01 $\pm$ .17	1.16 $\pm$ .19
T-learner	1.57 $\pm$ .32	1.71 $\pm$ .40	1.45 $\pm$ .25	1.49 $\pm$ .27	1.89 $\pm$ .47	1.96 $\pm$ .50
CEVAE	0.83 $\pm$ .17	0.85 $\pm$ .17	1.18 $\pm$ .15	1.36 $\pm$ .18	0.96 $\pm$ .12	0.98 $\pm$ .12
CFR	0.94 $\pm$ .10	0.98 $\pm$ .12	1.10 $\pm$ .20	1.18 $\pm$ .20	2.09 $\pm$ .45	2.17 $\pm$ .48
GANITE	0.88 $\pm$ .15	0.97 $\pm$ .15	1.60 $\pm$ .36	1.67 $\pm$ .34	2.48 $\pm$ .39	2.59 $\pm$ .47

Compared with the averaged RMSE over all POs generated by PO-Flow in Table 1, selecting the most likely POs based on log-density yields smaller RMSEs, providing more confident and closer estimates.

## D.3 Convergence and Computational Costs

Figure 3 shows the convergence of RMSE on multiple datasets. PO-Flow demonstrates rapid convergence across datasets, requiring only around 250 training iterations (not epochs) with a batch size of 200 per iteration. This highlights the model’s strong training efficiency.

In addition, Table 9 compares model size, training time to convergence, and sampling time (for 500 samples) across PO-Flow and other deep generative baselines. All experiments were conducted on a single A100 GPU. Notably, PO-Flow attains superior results with the fewest neural network

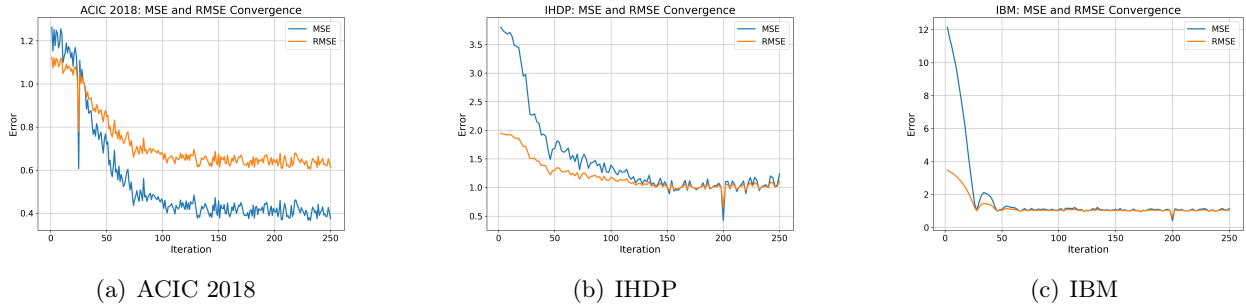


Figure 3: Convergence of MSE and RMSE for predicted potential outcomes over the training iterations on the ACIC 2018, IHDP, and IBM datasets.

Table 9: Comparison of model size, training time until convergence, and sampling cost (for 500 samples).

Methods	# Params	Training Time	Sampling
<b>PO-Flow</b>	32,394	<b>0.96min</b>	<b>0.58s</b>
DiffPO	176,372	5.75min	4.98s
INFs	138,172	5.09min	0.74s
GANITE	167,381	4.93min	0.80s
CEVAE	97,864	4.64min	0.47s

parameters, leading to faster training and substantially reduced sampling time compared with diffusion-, discrete flow-, and GAN-based methods.